

Increasing the performance of energy harvesting in vibration mode shapes

Majid Jabbari^{*}, Mostafa Ghayour^a and Hamid Reza Mirdamadi^b

Department of Mechanical Engineering, Isfahan University of Technology, Isfahan 84156-83111, Iran

(Received December 21, 2015, Revised January 28, 2016, Accepted February 11, 2016)

Abstract. This paper presents a method of design for the energy harvesting of a piezoelectric cantilever beam. Vibration modes have strain nodes where the strain distribution changes in the direction of the beam length. Covering the strain nodes of the vibration modes with continuous electrodes effects a cancellation of the voltages outputs. The use of segmented electrodes avoids cancellations of the voltage for multi-mode vibration. The resistive load affects the voltage and generated power. The optimum resistive load is considered for segmented and continuous electrodes, and then the power output is verified. One of the effective parameters on energy harvesting performance is the existence of concentrated mass. This topic is studied in this paper. Resonance and off-resonance cases are considered for the harvester. In this paper, both theoretical and experimental methods are used for satisfactory results.

Keywords: energy harvesting; strain nodes; generated power; vibration modes

1. Introduction

Energy harvesting of structural vibration is useful for electrical devices. Research and studies have shown the importance of this subject. Harvesting is suitable for generating power and it can be applied to devices and rechargeable batteries. Energy harvesting is used in structural health monitoring and wireless sensors. Some of research has focused on dimensions, material parameters, and the effect of shape on the performance of piezoelectric energy harvesting.

Renno *et al.* (2009) suggested a procedure to maximize the energy harvesting of a vibration source by optimization of the parameters of the structures. They presented an analysis of the power generated from the energy harvesting of piezoelectric systems. Gammatori *et al.* (2010) proposed a method to maximize the harvested energy for a range of excitation frequencies. Elvin *et al.* (2003) concluded that a load from a roller cart can generate mechanical strains for energy harvesting. He applied this subject for the implementation of damage detection. Nuffer and Bein (2006) explained the energy harvesting application to generated power for a wireless sensor. Granstrom *et al.* (2007) discussed the power generated from oscillating tension of a strap of piezoelectric polymer. Leland *et al.* (2004) used the energy harvesting of a device to generate

^{*}Corresponding author, Ph.D. Student, E-mail: jabbari_nik@yahoo.com

^aProfessor, E-mail: ghayour@cc.iut.ac.ir

^bAssociate Professor, E-mail: harmirdamadi@cc.iut.ac.ir

electrical power from the vibration of a staircase. Jeon *et al.* (2005) applied a thin film piezoelectric generator for Micro-Electro-Mechanical System devices. Zheng *et al.* (2009) used a configuration optimization method for energy harvesting of a piezoelectric beam by the energy conversion factor. The electric circuitry and the static load are the limitation of this study. Ertruck and Inman (2008) proposed single degree of freedom modeling and distributed modeling for the energy harvesting of a cantilever beam through corrections to the models. Shen *et al.* (2007) verified the energy harvesting performance of various kinds of piezoelectric materials. Lee *et al.* (2009) presented a new conceptual design for the energy harvesting of a piezoelectric beam to apply multiple vibration modes with a segmented piezoelectric structure. Another parameter for the verification of energy harvesting performance is electrical circuitry. Ottman *et al.* (2002) researched the effect of a converter to maximize the generated power of a piezoelectric device. Guan and Liao (2007) showed the effect of energy harvesting circuits on storage voltage. Rupp *et al.* (2009) presented a design method for the energy harvesting of a piezoelectric shell with the parameters of piezoelectric material and a resistive load on the electric circuit.

Previous research has been focused on geometry, material parameters, and electrical circuitry for maximizing of the energy harvesting of a piezoelectric structure. Another parameter for harvesting the energy of piezoelectric beams is the existence of the strain nodes in the vibration mode shape. Crawley and Luis (1987) explained the effect of strain nodes on the performance of the actuator. According to their research, the position of the actuator must be away from these points. Otherwise the force produced by the actuator will be decreased, since one section of the actuator will be opposing the other. Therefore, it is necessary to use segmented actuators for controlling flexible structures.

The vibration modes of a cantilevered beam have strain nodes where strain distribution changes in the direction of the beam length. In this paper, it is demonstrated that covering the strain nodes of the vibration modes with continuous electrodes effects cancellation of voltage output. The use of segmented electrodes avoids cancellation of the voltage for multi-mode vibration.

A bimorph cantilevered beam is used in both the continuous electrode example and the segmented electrode example. The effect of the concentrated mass at the tip of the beam is also considered. The behavior of the harvester is verified in both resonance and off-resonance situations.

2. Theoretical formulation

Fig. 1 shows the bimorph beam with the substructure and electrical circuit. The circuit equation of a piezoelectric layer and an electric current are expressed by Gauss's law

$$\frac{d}{dt} \left(\int_A D \cdot n dA \right) = \frac{v(t)}{R_l} \quad (1)$$

Where D is the vector of electric displacement. R_l is the resistive load, v is the electric potential, n is the unit normal, and A is the electrode area.

The electrode covers piezoelectric the layers perpendicularly in 3-directions, so that the $D_3 n_3$ component is the result of inner product $D \cdot n$ in Eq. (1).

The axial strain is proportional to the curvature of the beam at level 'z' according to Eq. (2).

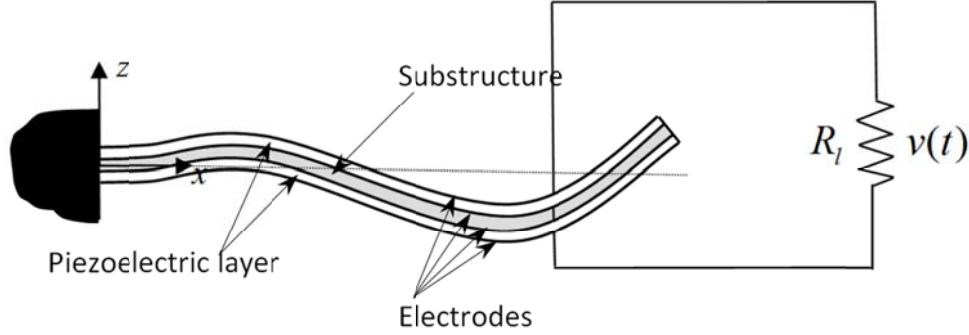


Fig. 1 The bimorph beam with substructure and electrical circuit

$$s_1(x, z, t) = -z \frac{\partial^2 w(x, t)}{\partial x^2} \quad (2)$$

Where s_1 is the axial strain and w is the transverse displacement of the beam. The electric field is obtained with Eq. (3)

$$\begin{cases} E_{3t}(t) = \frac{-v(t)}{h_p} & \text{in top layer of the parallel connection} \\ E_{3b}(t) = \frac{v(t)}{h_p} & \text{in bottom layer of the parallel connection} \\ E_3(t) = \frac{-v(t)}{2h_p} & \text{in both layers of the series connection} \end{cases} \quad (3)$$

Where E_3 , is the electric field, and h_p , is thickness of the piezoelectric layer. By using the piezoelectric constitutive relationship Eq. (4), Eq. (2) and Eq. (3) in Eq. (1), the following equation Eq. (5) is obtained

$$D_3 = e_{31}s_1 + \varepsilon_{33}^s E_3 \quad (4)$$

$$C_p^{eq} \frac{dv(t)}{dt} + \frac{v(t)}{R_l} = -e_{31} \frac{h_p}{2} b \int_0^L \frac{\partial^3 w_{rel}(x, t)}{\partial x^2 \partial t} dx \quad C_p^{eq} = \varepsilon_{33}^s \frac{bL}{2h_p} \quad (5)$$

Where e_{31} is the piezoelectric coefficient, ε_{33}^s is the dielectric coefficient, s_1 is strain, C_p^{eq} is the equivalent electric capacitance, b is the width of the piezoelectric layer, L is the length of the piezoelectric layer, and w_{rel} is transverse displacement.

The modal expansion form of the transverse vibration response can be substituted in Eq. (5)

$$w(x, t) = \sum_{r=1}^{\infty} \phi_r(x) \tau_r(t) \quad (6)$$

Table 1 The equations of θ_r and C_p^{eq}

Connection	θ_r	C_p^{eq}
Parallel	$-e_{31} h_p b \left. \frac{d\phi_r(x)}{dx} \right _{x=L}$	$\frac{2\varepsilon_{33}^S bL}{h_p}$
Series	$-e_{31} \frac{h_p}{2} b \left. \frac{d\phi_r(x)}{dx} \right _{x=L}$	$\frac{\varepsilon_{33}^S bL}{2h_p}$

$$C_p^{eq} \frac{dv(t)}{dt} + \frac{v(t)}{R_l} = \sum_{r=1}^{\infty} \theta_r \frac{d\tau_r(t)}{dt} \quad (7)$$

$$\theta_r = a \int_0^L \frac{d^2\phi_r(x)}{dx^2} dx = a \left. \frac{d\phi_r(x)}{dx} \right|_{x=L}$$

Where θ_r is the current parameter, that is a function of the geometric, material, and piezoelectric coupling parameters and the bending slope Eigen function at the boundaries of the electrodes. θ_r and C_p^{eq} are expressed according to Table 1.

$\frac{d\phi_r(x)}{dx}$ is the modal velocity response, which changes according to the voltage response. If the electrodes cover a region over the piezoceramic, θ_r is expressed as

$$\theta_r = -e_{31} \frac{h_p}{2} b \left. \frac{d\phi_r(x)}{dx} \right|_{x_s}^{x_e} \quad (8)$$

According to Eq. (8), the electromechanical coupling term depends on the locations of the electrodes.

By exciting the structure harmonically at a certain natural frequency, ω_r , Eq. (7), is expressed as follows

$$C_p^{eq} \frac{dv(t)}{dt} + \frac{v(t)}{R_l} = \theta_r A_r e^{j\omega_r t} \quad (9)$$

Where $A_r e^{j\omega_r t}$ is the modal velocity response. That is the function of the voltage response given by $v(t)$. Therefore the exciting electrical circuit depends on the respective mode shape.

By using Eq. (10) in the equation of motion and electromechanical equation, Eqs. (11) and (12) are obtained (Ertruck and Inman 2008)

$$\tau_r(t) = H_r e^{j\omega t} \quad v(t) = V e^{j\omega t} \quad A_r = j\omega H_r \quad (10)$$

$$(\omega_r^2 - \omega^2 + j2\zeta_r \omega_r \omega) H_r + \theta_r V = F_r \quad (11)$$

$$\left(\frac{1}{R_l} + j\omega C_p^{eq} \right) V - j\omega \sum_{r=1}^{\infty} \theta_r H_r = 0 \quad (12)$$

$$F_r = 2\rho b h_p a_d \quad a_d = d\omega^2 \quad (13)$$

Where a_d , is the excitation acceleration amplitude, ω is the excitation frequency, t is time, ρ is density, d is the translate displacement amplitude of the clamp, V is voltage amplitude, and H_r is the time function amplitude.

According to Eq. (8), the bending slopes at the boundaries of the electrodes are the effective parameter in energy harvesting. For a certain mode shape, if the bending slopes at the boundaries of the electrodes are close to each other, the electrical output is low. The reason for this problem is the strain distribution in the length of the structure. If the sign of the strain distribution changes, cancellation of the electrical output from energy harvesting is obtained for a certain vibration mode.

The Eigen curvature function in Eq. (7) shows the cancellation conditions. The positive and negative areas under the Eigen curvature function, by integrating electric displacement over the electrode area, reduce electrical output. Thus, integration over the segmented electrode areas can avoid the phenomenon of cancellation. The position of the sign change of the curvature is called the strain node. The bending strain depends on the curvature at one point of the thin beam, so the inflection points of the Eigen function are the strain nodes for the vibration mode.

A cantilevered beam based on the Euler Bernoulli theory is considered for the position of the dimensionless strain nodes. The result of the normalized Eigen function of the vibration mode for the short circuit condition is expressed as

$$\phi(x) = \sqrt{\frac{1}{mL}} \left[\cosh \frac{\lambda_r}{L} x - \cos \frac{\lambda_r}{L} x - \sigma_r \left(\sinh \frac{\lambda_r}{L} x - \sin \frac{\lambda_r}{L} x \right) \right] \quad (14)$$

$$\sigma_r = \frac{\sinh \lambda_r - \sin \lambda_r}{\cosh \lambda_r + \cos \lambda_r} \quad (15)$$

The eigenvalue of the vibration mode (λ_r) is obtained by Eq. (16)

$$1 + \cos \lambda \cosh \lambda = 0 \quad (16)$$

The positions of the strain nodes are the basis of the following equation

$$\cosh \lambda_r \bar{x} + \cos \lambda_r \bar{x} - \sigma_r (\sinh \lambda_r \bar{x} + \sin \lambda_r \bar{x}) = 0 \quad \bar{x} = \frac{x}{L} \quad (17)$$

The undamped natural frequencies of the cantilever piezoelectric beam in the short circuit state are obtained with the following equation

$$\omega_r = \lambda_r^2 \sqrt{\frac{YI}{mL^4}} \quad m = b(\rho_s h_s + 2\rho_p h_p) \quad YI = \frac{2b}{3} \left[Y_s \frac{h_s^3}{8} + c_{11}^E \left(\left(h_p + \frac{h_s}{2} \right)^3 - \frac{h_s^3}{8} \right) \right] \quad (18)$$

Where Y_s is the elastic module of the substructure, h_s , is thickness of the substructure, c_{11}^E is

elastic modulus of the piezoelectric layer, ρ_s and ρ_p are density of the substructure and the piezoelectric layer, respectively.

Table 2 shows the positions of the strain nodes for the cantilevered beam without a tip mass in the short circuit state. According to the results, the number of strain nodes is one unit less than the number of vibrations. Figs. 2 and 3 show the normalized displacement mode shapes and the strain mode shape of the cantilevered beam.

Table 2 The position of the strain nodes for the cantilevered beam without a tip mass in the short circuit

Mode number	eigenvalue	The first strain node	The second strain node	The third strain node	The fourth strain node
1	1.87510407	-	-	-	-
2	4.69409113	0.2165	-	-	-
3	7.85475744	0.1323	0.4965	-	-
4	10.9955407	0.0944	0.3559	0.6417	-
5	14.1371684	0.0735	0.2768	0.5001	0.7212

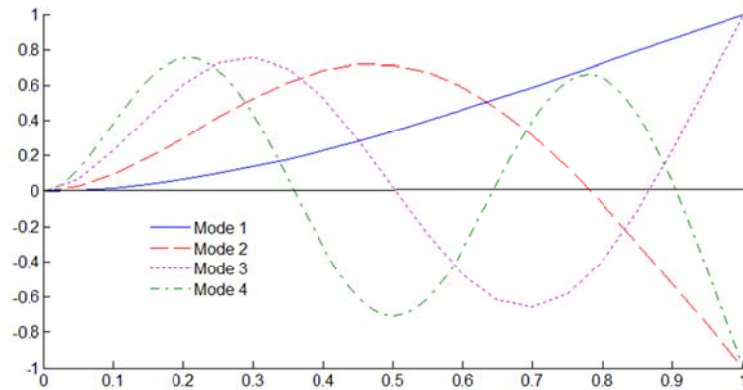


Fig. 2 The normalized displacement mode shapes

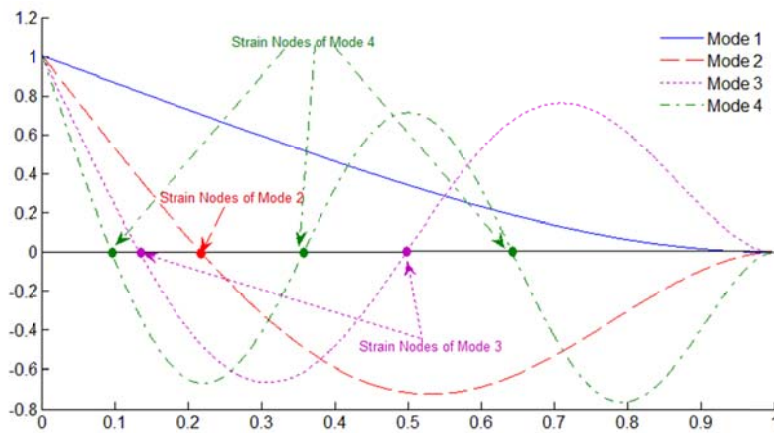


Fig. 3 The strain mode shape of the cantilevered beam

If a concentrated mass (M) is attached to the tip of the cantilevered beam, the eigen function is presented as follows

$$\phi(x) = \sqrt{\frac{1}{mL}} \left[\cosh \frac{\lambda_r}{L} x - \cos \frac{\lambda_r}{L} x - \sigma_r \left(\sinh \frac{\lambda_r}{L} x - \sin \frac{\lambda_r}{L} x \right) \right] \quad (19)$$

$$\sigma_r = \frac{\sinh \lambda_r - \sin \lambda_r - \lambda_r \frac{M}{mL} (\cos \lambda_r - \cosh \lambda_r)}{\cosh \lambda_r + \cos \lambda_r - \lambda_r \frac{M}{mL} (\sin \lambda_r - \sinh \lambda_r)} \quad (20)$$

The eigenvalue of the beam with a concentrated mass is expressed by Eq. (21)

$$1 + \cos \lambda \cosh \lambda + \lambda * M * (\cos \lambda \sinh \lambda - \sin \lambda \cosh \lambda) = 0 \quad (21)$$

Table 3 The eigenvalue of the first three modes for a cantilevered beam with the concentrated mass

Mass ratio(M/mL)	The first eigenvalue	The second eigenvalue	The third eigenvalue
0	1.875	4.694	7.854
0.1	1.722	4.399	7.451
0.2	1.616	4.267	7.318
0.24	1.582	4.233	7.288
0.3	1.536	4.192	7.253
0.4	1.472	4.144	7.215
0.5	1.419	4.111	7.19
0.6	1.375	4.086	7.172
0.7	1.337	4.067	7.159
0.8	1.304	4.053	7.148
0.9	1.274	4.041	7.14
1	1.247	4.031	7.134

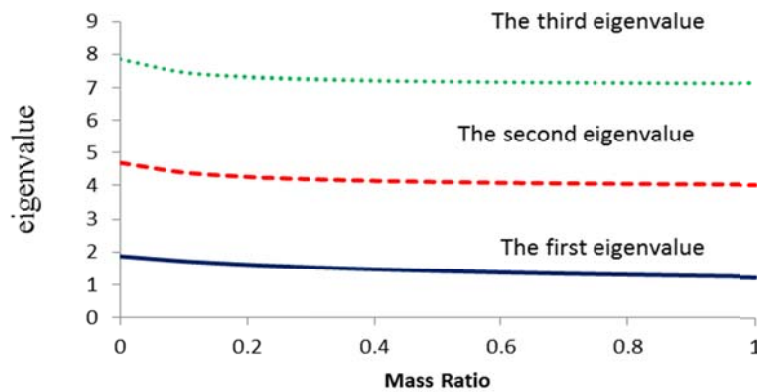


Fig. 4 The eigenvalue versus parameter of mass ratio

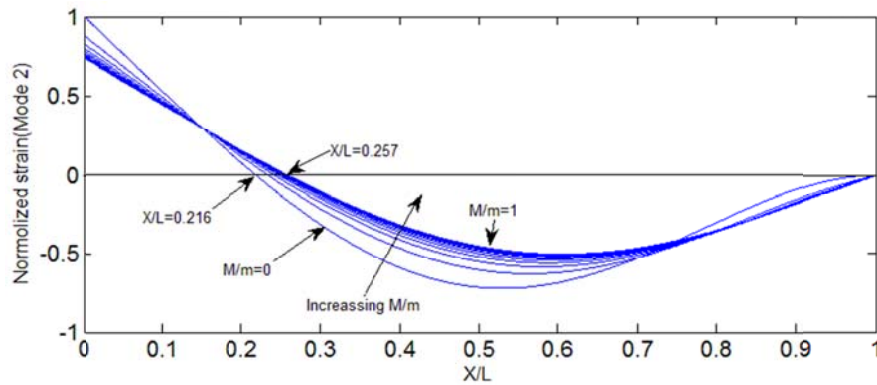


Fig. 5 The strain mode shape of the second vibration modes for the change of mass ratio

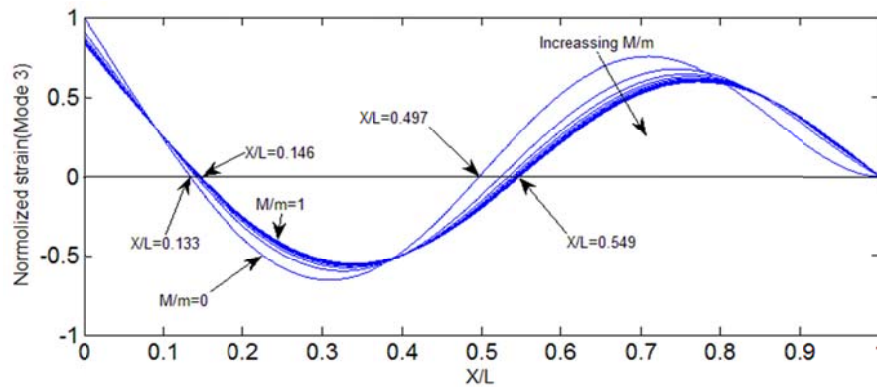


Fig. 6 The strain mode shape of the third vibration modes for the change of mass ratio

Table 3 shows the eigenvalue of the first three modes for the cantilevered beam with the concentrated mass. The variation of the eigenvalue versus the parameter of the mass ratio (concentrated mass relative to the beam mass) is given in Fig. 4. According to figure, the eigenvalues decrease with the increasing mass ratio. Consequently, the position of the strain nodes depends on the value of the mass ratio. The strain node shapes of the second and third vibration modes for the change in mass ratio are displayed in Figs. 5 and 6.

According to figure, as the mass ratio increases, the position of the strain nodes in the second and third modes moves to the tip of beam.

Power and generated electrical voltage are obtained by using the optimum resistive load (Xu *et al.* 2013).

3. Specimen under test and experimental setup equipment

In the case of the series connection, the piezoelectric structure used is a bimorph beam. The specimen was obtained from Ultrasonic Science and Technology Company. Its properties were presented by its manufacturer. The length, width, and thickness of the bimorph are 40 mm, 7.1 mm, and 0.76 mm, respectively. The properties of the dimensions and the material of the specimen

are shown in Tables 4 and 5. The first three vibration modes are used to verify the voltage cancellation phenomenon. There is no voltage cancellation in the first vibration mode, and this phenomenon occurs at higher modes of excitation.

The position of the strain nodes are $0.2165L$ for the second mode and $0.1323L$ and $0.4965L$ for the third mode. So the distance of these strain nodes are approximately 8.66mm, 5.292mm, and 19.86mm from the clamped end of the beam (Fig. 7). The continuous electrodes are cut at the position of the strain nodes by Nitric Acid in the specimen. Therefore, the piezoelectric beam is divided to four parts. To verify the energy harvesting, a resistive load is used for each part. The combination voltages are obtained by a rectifier.

The cantilever beam used is a bimorph. The experimental equipment setup used is shown in Fig. 8. A potentiometer is used to obtain the resistance load. The harmonic excitation applied by the shaker to the base of the beam is given in Eq. (10). The excitation acceleration amplitude applied is 45 m/s^2 . The dimension properties of the segmented electrodes are presented in Fig. 7. The experimental results in the modal test show natural frequency values of 263.5, 1361, and 4751 Hz for the condition without a concentrated mass, and 142, 1100, and 4157 Hz in the case of the existence of a concentrated mass. Table 6 shows the results of frequency in both the experimental and numerical methods. An open circuit is considered to verify the voltage response in the resonance frequencies. The resistive load of the open circuit selected is $1 \text{ M}\Omega$.

Table 4 The properties material of specimen

$c_{11}^E = 66.67 \times 10^9 \text{ (N / m}^2\text{)}$
$d_{31} = -210 \times 10^{-12} \text{ (m / V)}$
$\epsilon_{33}^s = 21.249 \times 10^{-9} \text{ (F / m)}$
$\rho = 7800 \text{ (kg / m}^3\text{)}$

Table 5 The properties of dimensions of specimen

L(mm)	b(mm)	h_p (mm)
40	7.1	0.76

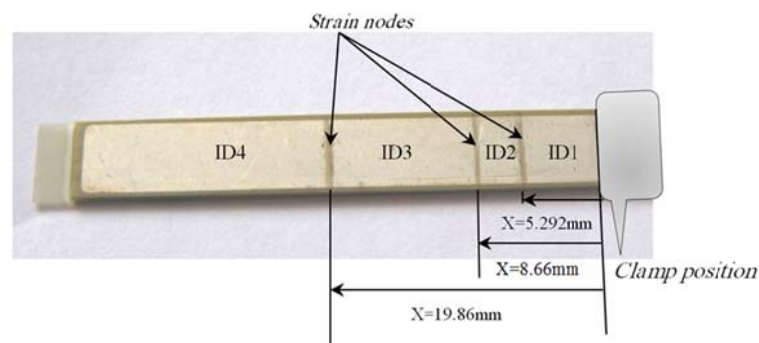


Fig. 7 The position of the strain nodes and the segmented electrodes

Table 6 The results of frequency in experimental and numerical methods

Frequency mode	Frequency value (Hz)(case of without the concentrated mass)		Frequency value (Hz)(case of existence of the concentrated mass)	
	Experimental method	Numerical method	Experimental method	Numerical method
1	263.5	264.3	142	142.3
2	1361	1374	1100	1105
3	4751	4802	4157	4195

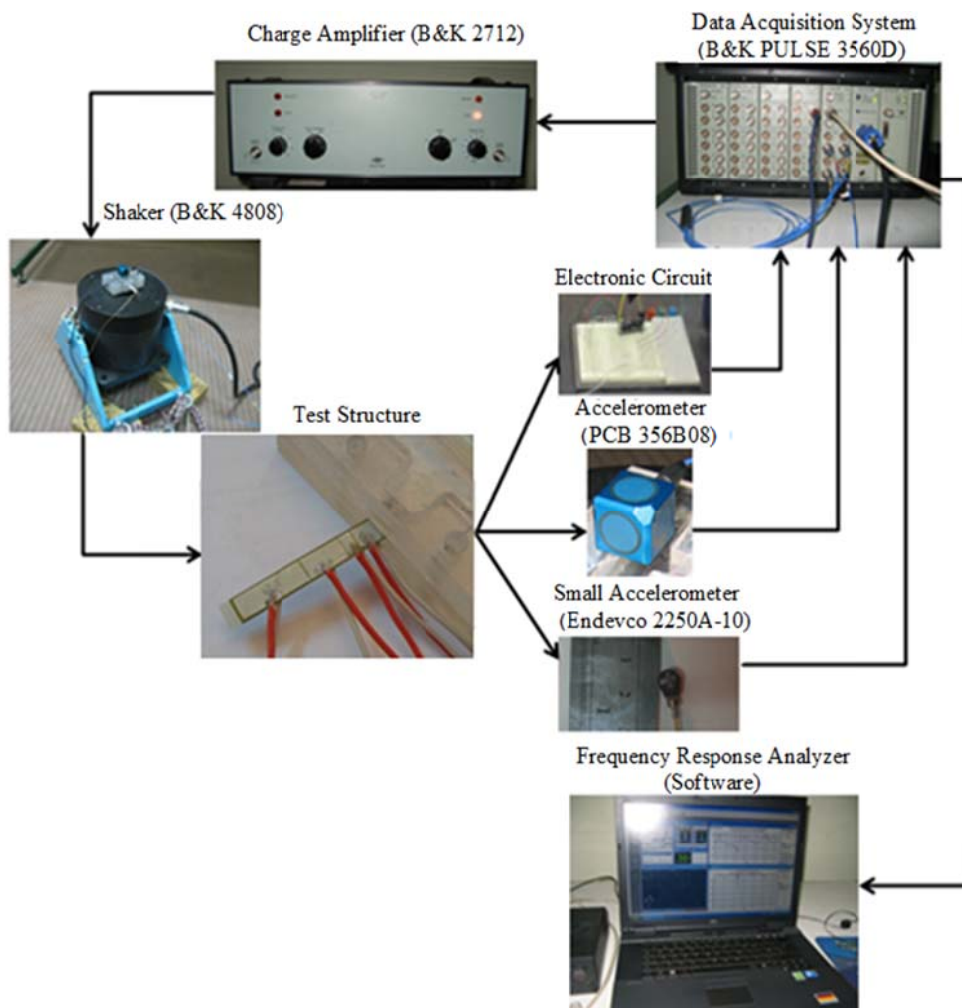


Fig. 8 The experimental setup equipment

4. Results of voltage response at resonance frequencies

If the beam is excited by the first vibration mode, a strain node will not be obtained over the length of the beam. In this case, the amplitude of the voltage response across the continued

electrode should be equal to the combined amplitude of the voltage responses across the segmented electrodes (ID 1, 2, 3, 4). The results of the amplitude of the voltage response are shown in Table 7 and Fig. 9. According to Fig. 10, the voltage amplitude of the continuous electrode is close to the segmented electrodes. The existence of a limited space between the segmented electrodes causes a slight difference in the amplitudes of the continuous electrode and segmented electrodes. However, the results show that continuous electrodes are suitable for energy harvesting in the first vibration mode.

Table 7 The results of the amplitude of the voltage response

ID	Voltage amplitude(mV) in the first mode	Voltage amplitude(mV) in the second mode	Voltage amplitude(mV) in the third mode
1	12.2	5.09	1.61
2	6.0	0.89	-0.49
3	14.3	-5.59	-3.3
4	8.1	-10.04	5.38
Continuous electrode	41.4	-9.65	3.2

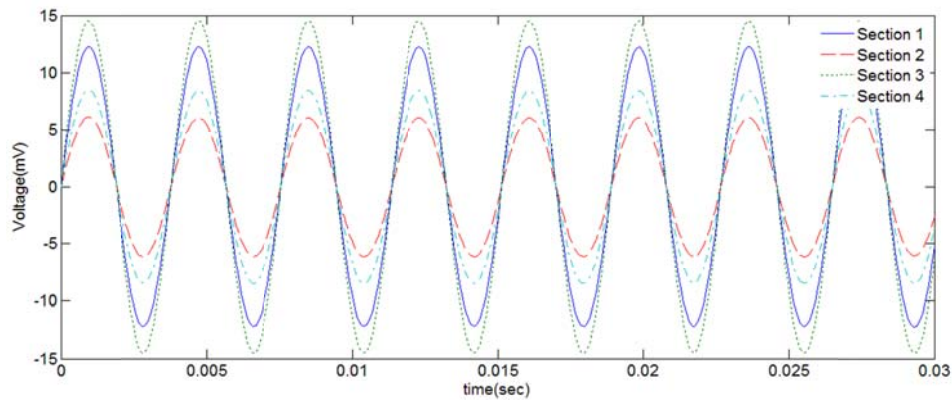


Fig. 9 The amplitude of the voltage response of the segmented electrodes at the first natural frequency

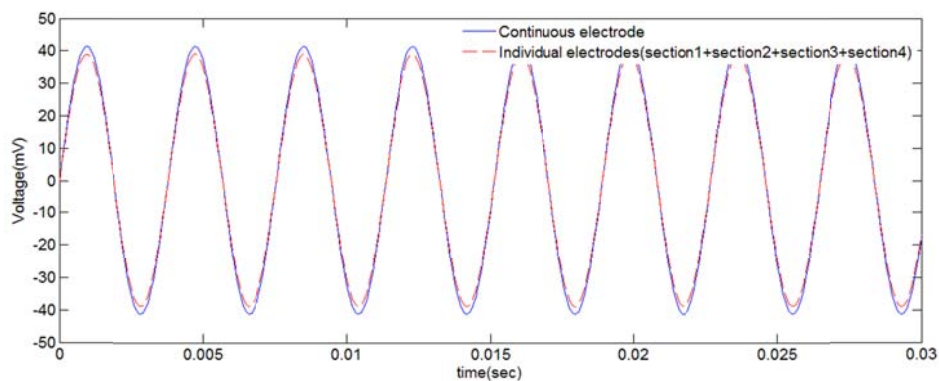


Fig. 10 The combined amplitude of the voltage response of the segmented electrodes and the continued electrode at the first natural frequency

If the piezoelectric beam vibrates at the second natural frequency, the strain node is obtained in the position of 8.66 mm according to Fig. 7. For this case, the voltage responses of the segmented electrodes are shown in Fig. 11. When the beam is excited at the second natural frequency, Sections 1 and 2 are in compression, Sections 3 and 4 are in tension, and vice versa. So the voltage of Sections 1 and 2 have a phase difference of 180 degrees with a voltage of Sections 3 and 4. Fig. 12 shows the voltage response of the continuous electrode and the segmented electrodes. In the case of the continuous electrode, the change in phase of voltage response in the strain node causes the cancellation phenomenon. The maximum voltage response is obtained from a combination of the voltage output at the sides of the strain node at a position of 8.66 mm considering the phase difference. According to the results, the combination of the voltage amplitude of the segmented electrodes is more than 2 times the voltage amplitude of continuous electrode.

If the piezoelectric beam vibrates at the third natural frequency, the strain nodes are obtained in positions of 0.94 mm and 3.5 mm. For this case, the voltage responses of the segmented electrodes are shown in Fig. 13. When the beam is excited at the third natural frequency, Sections 1 and 4 are

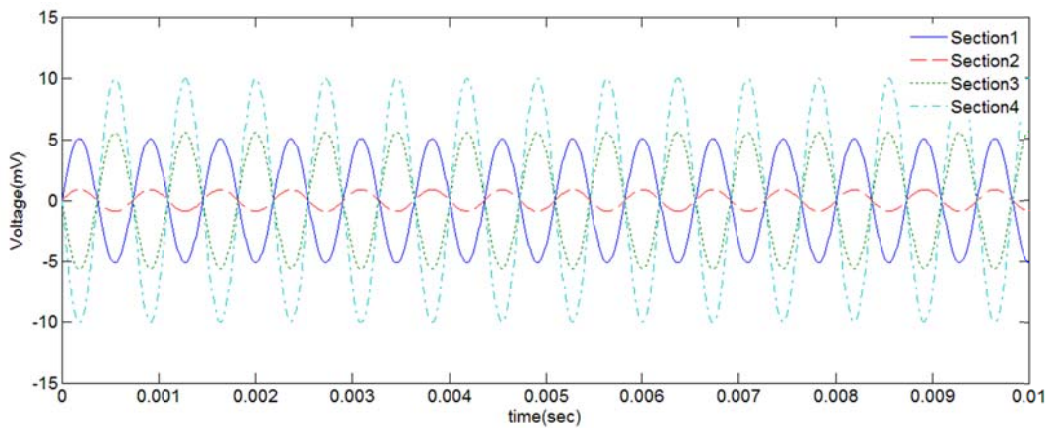


Fig. 11 The amplitude of the voltage response of the segmented electrodes at the second natural frequency

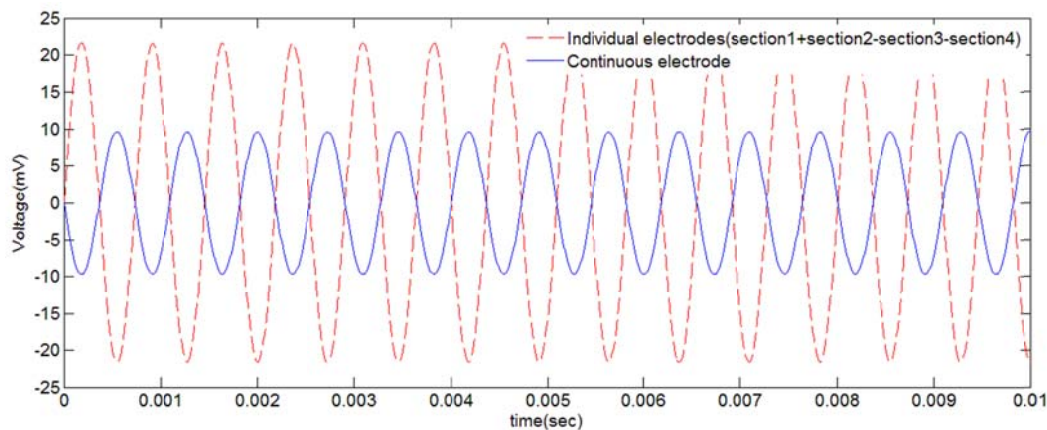


Fig. 12 The combined amplitude of the voltage response of the segmented electrodes and the continued electrode at the second natural frequency

in compression, Sections 2 and 3 are in tension, and vice versa. So the voltage of Sections 1 and 4 have a phase difference of 180 degrees with the voltage of Sections 2 and 3. Fig. 14 shows the voltage response of the continuous electrode and the segmented electrodes for excitation at the third natural frequency. The maximum voltage response is obtained from the combination the voltage output at the sides of the strain nodes at positions of 0.94 mm and 3.5 mm considering the phase difference. According to the results, the combination of the voltage amplitudes of the segmented electrodes is more than 3.3 times the voltage amplitude of the continuous electrode. The voltage response of the continuous electrode is less than the combination of voltage responses of the segmented electrodes. Hence, the continuous electrode is not suitable for excitation at second and third natural frequencies.

The existence of a concentrated mass at the tip of beam has an effect on the positions of the strain nodes. The concentrated mass is considered to be 0.4 gr. The positions of the strain nodes are 0.2427L for the second mode and 0.1436L and 0.5369L for the third mode. Consequently, the distances of these strain nodes are approximately 9.68 mm, 5.744 mm, and 21.48 mm from the

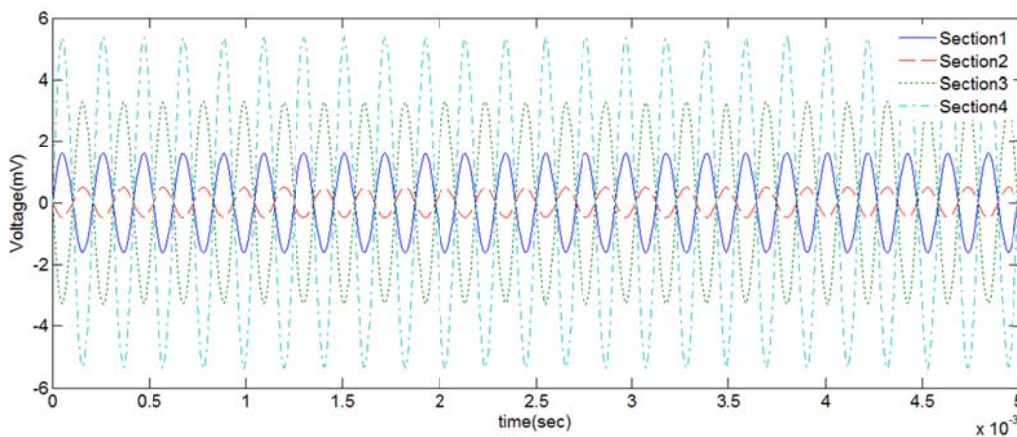


Fig. 13 The amplitude of the voltage response of the segmented electrodes at the third natural frequency

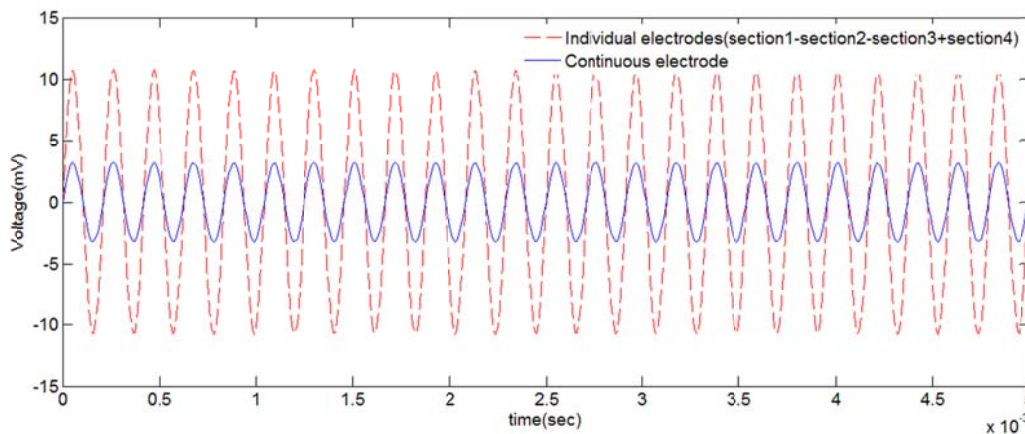


Fig. 14 The combined amplitude of the voltage response of the segmented electrodes and the continued electrode at the third natural frequency

Table 8 The dimensions and the electrical capacitance of the divided electrodes

ID	\bar{x}	B(mm)	b(mm)	h_p (mm)	C_s (nF)
1	0.1436	5.744	7.1	0.38	22.8
2	0.2427	3.964	7.1	0.38	1.574
3	0.5369	11.768	7.1	0.38	4.673
4		18.524	7.1	0.38	7.354

Table 9 The voltage responses of the segmented electrodes and continuous electrode for the existence of concentrated mass at the tip of beam

ID	Voltage amplitude(mV) in the first mode	Voltage amplitude(mV) in the second mode	Voltage amplitude(mV) in the third mode
1	3.15	2.149	1.21
2	1.69	0.407	-0.4
3	3.62	-2.29	-2.39
4	1.85	-3.59	3.405
Continuous electrode	9.8	-3.75	2.2

clamped end of the beam. Table 8 shows the dimensions and the electrical capacitance of the divided electrodes. The voltage responses are expressed in Table 9. The existence of a concentrated mass at the tip of the beam decreases the voltage response for the first three natural frequencies.

Although the existence of the concentrated mass effects the location of the strain nodes, the voltage ratio (the voltage combination of segmented electrodes per the voltage of continuous electrode) does not change for the second and third natural frequencies.

5. Results of generated power and voltage at off-resonant frequencies

In this case, electrical energy is delivered to a resistive load. In the off-resonance case, the excitation frequency is considered to be far from the resonance frequency. The first off-resonant frequency is selected 240 Hz, which is less than the first natural frequency. The second off-resonant frequency selected is 1250 Hz, which is less than the second natural frequency. The third off-resonant frequency selected is 4350 Hz, which is less than the third natural frequency. The output voltage and power depend on the resistance load. The optimum resistance changes according to the energy loss factor (Xu *et al.* 2013). The results of the power generated at the optimum resistive load are shown in Tables 10, 11, and 12 for both the continuous and the segmented electrodes at the first off-resonance frequency. According to the results, the power generated with the continuous electrode is more than 14 times the power generated from the segmented electrodes at the optimum resistive load at the first frequency. The power generated from the continuous electrode is more than 1.4 times the power generated from the segmented electrodes at the optimum resistive load at the second frequency. The power generated from the segmented electrodes is more than 1.7 times the power generated from the continuous electrode at the optimum resistive load at the third frequency.

Table 10 The results of the generated power in the optimum resistive load at the first off-resonance frequency

Method	ID	B	Voltage amplitude in the frequency 240Hz (mV)	Resistive load in the frequency 240Hz (Ω)	Electrical capacitance of the series connection C_s (nF)	Maximum power in the frequency 240 Hz $*10^{-11}$ (W)	The total power in the frequency 240Hz $*10^{-11}$ (W)
Segmented electrodes	1	5.292	1.275	631597.3	1.05	0.065	0.3825
	2	3.386	0.632	986870.8	0.672	0.01	
	3	11.182	1.51	298880.6	2.22	0.19	
	4	20.14	0.881	165794.3	4	0.1175	
Continuous electrode	-		4.3	83523.6	7.94	5.534	5.534

Table 11 The results of the generated power in the optimum resistive load at the second off-resonance frequency

Method	ID	Voltage amplitude in the frequency 1250Hz (mV)	Resistive load in the frequency 1250Hz (Ω)	Maximum power in the frequency 1250 Hz $*10^{-11}$ (W)	The total power in the frequency 1250Hz $*10^{-11}$ (W)
Segmented electrodes	1	0.528	121266.5	0.06	1.07
	2	0.093	189478.9	0.0012	
	3	-0.58	57355.9	0.146	
	4	-1.04	31832.5	0.86	
Continuous electrode	-	1	16036.6	1.55	1.55

Table 12 The results of the generated power in the optimum resistive load at the third off-resonance frequency

Method	ID	Voltage amplitude in the frequency 4350Hz (mV)	Resistive load in the frequency 4350Hz (Ω)	Maximum power in the frequency 4350 Hz $*10^{-11}$ (W)	The total power in the frequency 4350Hz $*10^{-11}$ (W)
Segmented electrodes	1	0.167	34846.5	0.02	1.04
	2	-0.0512	54447.7	0.0012	
	3	-0.341	16481.5	0.18	
	4	0.555	9147.3	0.842	
Continuous electrode	-	0.33	4608.2	0.591	0.591

The voltage amplitude of the segmented electrodes (ID 1, 2, 3, and 4) are shown in Fig. 15 for

excitation frequencies of 240, 1250, and 4350 Hz. According to the figure, the highest voltage output at a frequency of 240 is in the segmented Electrode 3, and the greatest value is in the segmented Electrode 4 for frequencies of 1250 and 4350 Hz. The reason for this is the curvature of the segmented electrodes into mode shapes.

Fig. 16 shows comparison the voltage amplitudes of the continuous electrode and the segmented electrodes for excitation frequencies of 240, 1250 and 4350 Hz. The results show the voltage outputs are the same for the first frequency 240 Hz. The voltage output of the segmented electrodes is greater than that of the continuous electrode for the second and third frequencies.

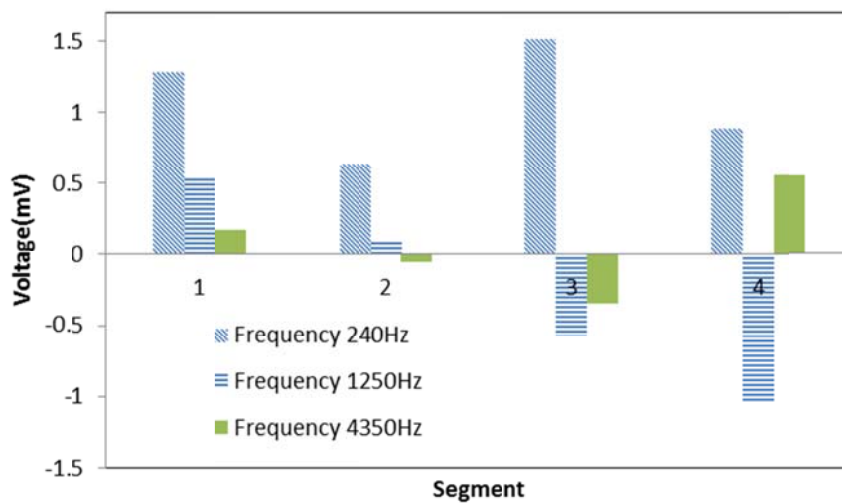


Fig. 15 The voltage amplitude of segment electrodes (ID1, 2, 3, 4) for the excitation frequencies of 240, 1250 and 4350 Hz

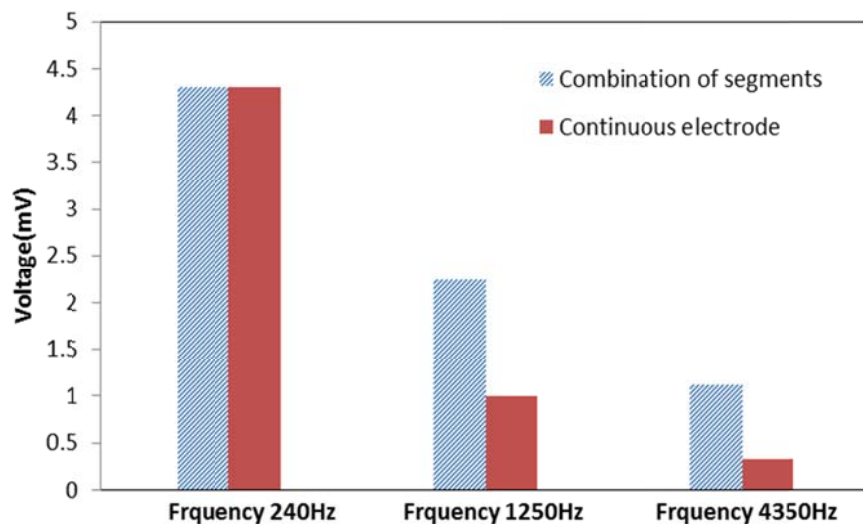


Fig. 16 The voltage amplitudes of the continues electrode and the segmented electrodes for excitation frequencies of 240, 1250 and 4350 Hz

Fig. 17 shows the power generated from the segmented electrodes (ID1, 2, 3, and 4) for frequencies of 240, 1250, and 4350 Hz. The results show the greatest power generated is in segmented Electrode 3 at a frequency of 240 Hz. At frequencies of 1250 and 4350 Hz, the greatest power generated is in segmented Electrode 4. A comparison between the power generated from the continuous electrode and the combination of segmented electrodes is shown in Fig. 18.

Note that excitation of the beam at the off-resonance frequency affects the position of the strain nodes in comparison to the resonance frequency. As a result, it affects the voltage response of the segmented electrodes. However, the change in the positions of the strain nodes is disregarded in the research.

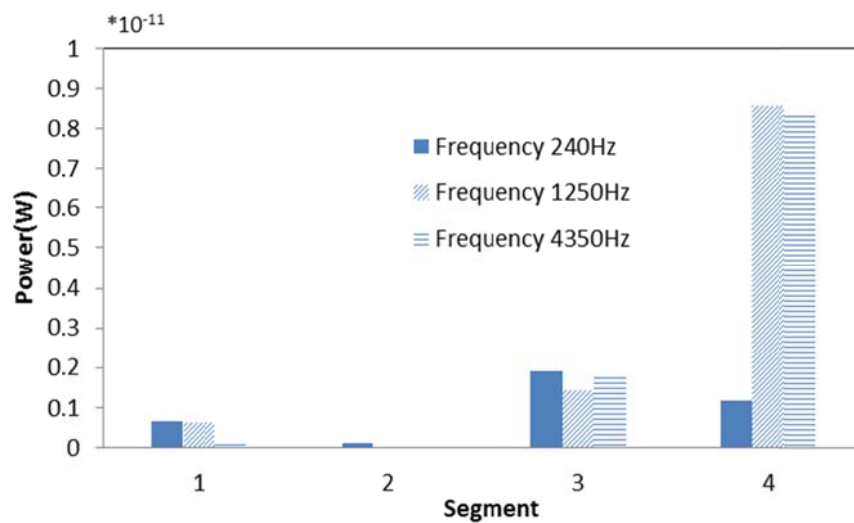


Fig. 17 The generated power of segmented electrodes (ID1,2,3,4) for frequencies of 240, 1250 and 4350 Hz

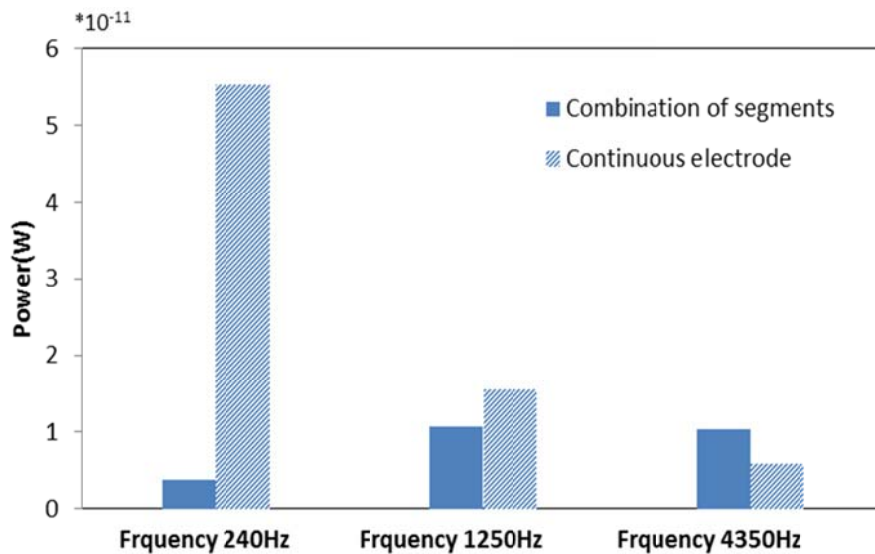


Fig. 18 The generated power between the continuous electrode and combination of segmented electrodes

6. Conclusions

In this paper the cancellation phenomenon in power and voltage response in the piezoelectric energy harvesting is discussed. The existence of strain nodes effects cancellation of the voltage output. The vibration modes all have strain nodes except for the first frequency number. A bimorph cantilevered beam was used in both the continuous electrode example and the segmented electrode example. The effect of a concentrated mass at the tip of the beam was also considered.

The behaviour of the harvester was verified in both resonance and off-resonance cases. In the case of excitation at the first natural frequency, the voltage response of the continuous electrode was comparable to that of the segmented electrodes in an open circuit state, while excitation at the second and third natural frequencies resulted in a decrease in the voltage output of the continuous electrode relative to the segmented electrode.

Although the existence of the concentrated mass effected the location of the strain nodes, the voltage ratio (the voltage of the segmented electrode per the voltage of the continuous electrode) did not change at the second and third natural frequencies.

The existence of a concentrated mass at the tip of the beam decreased the voltage response for the first three natural frequencies.

In the off-resonance case, the excitation frequency was considered to be far from the resonance frequency. A circuit with a resistive load was applied to verify energy harvesting. The maximum value of electric power was obtained at the optimum resistive load for the selected frequency value. Hence, the optimum resistive load was selected according to the excitation frequency and capacitance. Three of the excitation frequencies applied were lower than the first three natural frequencies.

The results demonstrated that the behaviour of the power generated in the off-resonance modes for the continuous electrode case and the segmented electrode case were different.

The power generated in the first off-resonance mode (lower than the first natural frequency) in the case of the continuous electrode was greater than that of the segmented electrode. In the second off-resonance mode (lower than the second natural frequency), the generated power for the continuous electrode case was comparable to that of the segmented electrode. In the third off-resonance mode (lower than the third natural frequency), the generated power for the continuous electrode case was less than that of the segmented electrode.

References

- Crawley, E.F. and Luis, J. (1987), "Use of piezoelectric actuators as elements of intelligent structured", *AIAA J.*, **25**(10), 1373-1385.
- Elvin, A. and Choi, D.H. (2003), "A self-powered damage detection sensor", *Strain Anal. Eng.*, **38**(2), 115-124.
- Erturk, A. and Inman, J. (2008), "Issues in mathematical modeling of piezoelectric energy harvesters", *Smart Mater. Struct.*, **17**(6), 065016.
- Gammaitoni, L., Neri, I. and Vocca, H. (2010), "The benefits of noise and nonlinearity: extracting energy from random vibrations", *Chemical Physics.*, **375**(2), 435-438.
- Granstrom, J., Feenstra, J., Sodano, A. and Farinholt, K. (2007), "Energy harvesting from backpack Instrumented with Piezoelectric Shoulder Straps", *Smart Mater. Struct.*, **16**(5), 1810-1820.
- Guan, M.J. and Liao, W.H. (2007), "On the efficiencies of piezoelectric energy harvesting circuits towards storage device voltages", *Smart Mater. Struct.*, **16**(2), 498-505.

- Jeon, Y.B., Sood, R., Jeong, J. and Kim, S.G. (2005), "MEMS power generator with transverse mode thin film PZT", *Sens. Actuator A.*, **122**(1), 16-22.
- Lee, S., Youn, B.D. and Jung, B.C. (2009), "Robust segment type energy harvester and its application to a wireless sensor", *Smart Mater Struct.*, **18**(9), 095021.
- Leland, E.S., Lai, E.M. and Wright, A. (2004), "A self-powered wireless sensor for indoor environmental monitoring", *Proceedings of WNCG Conference*, Aust in, TX.
- Nuffer, J. and Bein, T. (2006), "Application of piezoelectric materials in transportation industry", *Innovative Solutions for the Advancement of the Transport Industry*.
- Ottman, K., Hofmann, H.F., Bhatt, A.C. and Lesieutre, G.A. (2002), "Adaptive piezoelectric energy harvesting circuit for wireless remote power supply", *IEEE Trans. Power Elect.*, **17**(5), 669-676
- Renno, J.M., Daqaq, M.F. and Inman D.J. (2009), "On the optimal energy harvesting from a vibration source", *J. Sound Vib.*, **320**(1), 386-405.
- Rupp, C.J., Evgrafov, A., Maute, K. and Dunn, M. (2009), "Design of piezoelectric energy harvesting systems: A topology optimization approach based on multilayer plates and shells", *J. Intel. Mater. Syst. Struct.*, **20**(16), 1923-1939.
- Shen, D., Choe, S.Y. and Kim, D.J. (2007), "Analysis of piezoelectric materials for energy harvesting devices under high vibrations", *J. Appl. Phys.*, **46**(10A), 6755-6760.
- Xu, T.B., Siochi, E.J., Kang, J.H., Zuo, L., Zhou, W., Tang, X. and Jiang, X. (2013), "Energy harvesting using a PZT ceramic multilayer stack", *Smart Mater Struct.*, **22**(6), 065015.
- Zheng, B., Chang, C.J. and Gea, H.C. (2009), "Topology optimization of energy harvesting devices using piezoelectric materials", *Struct. Multidiscip. Optim.*, **38**(1), 17-23.